coatings

MDPI

Article

Correlation between Microstructure and Tribological Properties of Laser Surface Heat-Treated Stellite Coatings

Chang-Kyoo Park [1], Jung-Hoon Lee [2], Nam-Hyun Kang [2] and Eun-Joon Chun [3,*]

[1] Laser and Electron Beam Application Department, Korea Institute of Machinery and Materials, Daejeon 34103, Korea; ck0421@kimm.re.kr
[2] Department of Materials Science and Engineering, Pusan National University, Busan 46241, Korea; ljh898989@naver.com (J.-H.L.); nhkang@pusan.ac.kr (N.-H.K.)
[3] Department of Nano Materials Science and Engineering, Kyungnam University, Changwon 51767, Korea
* Correspondence: ejchun@kyungnam.ac.kr

Received: 10 April 2020; Accepted: 27 April 2020; Published: 28 April 2020

Abstract: To manufacture superior-performance continuous casting mold components, high-velocity oxygen fuel spraying of a Stellite-1 coating was followed by its laser heat treatment at 1373–1473 K using a diode laser. The effects of the laser irradiation conditions on the macro- and microstructural variations along with the hardness and wear resistance within the Stellite-1 coating were evaluated. After the heat treatment, micro-voids within the sprayed coating decreased in number slightly with an increase in the heat treatment temperature. The hardness of the sprayed Stellite-1 coating increased from that of the as-sprayed coating (680 HV) after the laser heat treatment, with a hardness of 860 HV obtained at 1473 K. The cause of the increase in hardness could be the formation of nano-sized W- and Cr-based carbides such as WC, M_7C_3, and $M_{23}C_6$, as suggested by transmission electron microscopy analysis. The tribological properties of as-sprayed and laser heat-treated samples were investigated by a pin-on-disk tribometer. The laser heat treatment of Stellite-1 coating enhanced wear resistance. This resulted in a lower coefficient of friction and wear rate for the laser heat-treated sample than those for the as-sprayed sample.

Keywords: Stellite; thermal spray coating; laser surface heat treatment; microstructure; wear resistance

1. Introduction

High-velocity oxygen fuel (HVOF) spraying is widely employed in the deposition of highly wear-resistant and corrosion-resistant protective coatings [1]. Stellite alloys are a group of Co-based superalloys that contain a high level (20–30 wt.%) of Cr, a moderate amount (4–18 wt.%) of W or Mo, and a specific amount (0.25–3 wt.%) of C; they are strengthened by the precipitation of carbides embedded in the cobalt solid solution matrix. These carbides provide excellent wear resistance to the Stellite alloys. In this regard, Stellite alloy powder has been largely employed in the HVOF spraying process [1] together with arc cladding [2,3], plasma transfer arc hardfacing [4], supersonic laser deposition [5], laser cladding [6–8], etc.

Throughout the steel production process, the production hardware is exposed to a combination of high temperatures, corrosive environments, and wear. This demanding and severe environment produces a broad range of degradation mechanisms and ultimately leads to deterioration in the product quality, reduced operating efficiencies, and high maintenance costs [9]. From among the available production hardware, the continuous casting mold is exposed to high-temperature abrasive wear environments. In other words, the casting mold wherein solidification of the molten steel is initiated experiences a large amount of high-temperature wear [9–11]. In particular, the continuous casting

mold is the core component of the continuous casting system, and the surface quality of the mold is highly correlated with the surface quality of the slab. It determines the production efficiency of the continuous casting machine. Therefore, it should be highly durable and undergo minimal mold surface damage. To this end, Cu molds have been electroplated with a Ni and Ni-B alloy, and in addition, a HVOF spray coating of a Stellite alloy was examined for further enhancement of the surface mechanical properties. However, even though several studies have investigated the HVOF spraying of Stellite alloys [12–16], relevant results concerning high-durability continuous casting molds have not been reported upon sufficiently.

As a general rule, post-coating heat treatment is usually necessary as HVOF spray coating results in an inhomogeneous microstructure distribution that creates voids in the coating [1,12,13,17]. Therefore, numerous studies have already examined the influence of the heat treatment itself as well as the conditions imposed by the treatment, on the mechanical and chemical properties of the HVOF sprayed coating [17–20]. Gil et al. reported that the hardness and corrosion resistance of a Ni-based HVOF sprayed coating improved after heat treatment in a furnace, resulting in a densification of the microstructure as well as reduced porosity compared to that of the as-sprayed coating [17]. Navas et al. also investigated the effect of the flame melting treatment on the wear properties of a Ni-based sprayed coating. After the flame melting process, the porosity decreased and the microstructure exhibited a homogeneous distribution. As a result, the hardness and wear properties of the material improved [18]. Especially in the case of the continuous casting molds investigated in this study (consisting of a Cu plate with an electroplated Ni alloy layer and a Stellite HVOF coating), the application of classical heat treatment (i.e., using a furnace) is extremely difficult owing to distortion and desquamation issues arising from the different thermal expansion coefficients and melting points of the constituent materials. Thus, a laser heat treatment process is required in the case of HVOF sprayed coating of the continuous casting mold, as lasers bypass these issues and offer several advantages such as selective and precise control of the surface properties [21].

In this regard, many researchers have investigated the laser-based surface treatment of several types of Stellite coating [14,15,21–25]. Ciubotariu et al. undertook the surface remelting of a Stellite-6 coating by a pulsed Nd:YAG laser and optimized the remelting conditions [14]. Houdková et al. also investigated the surface remelting behavior of a Stellite-6 coating using a diode laser, and they reported a homogeneously distributed microstructure and an enhanced sliding wear property, despite decreased hardness [15]. In other words, almost all such studies used the selective melting process with laser power and scan speed as the main parameters. One of the main possible disadvantages of this remelting concept of the coating is an inhomogeneous remelted depth (i.e., dilution with substrate) because of thermal storage during the laser irradiation. On the other hand, when compared to the results on selective melting, there is a paucity of results on heat treatment within the solid-state temperature range and on the heat treatment temperature that is maintained constant during the laser irradiation. This heat treatment temperature does not cause the Stellite coating to melt.

In this study, the HVOF coating of the Stellite alloy was employed to obtain a high-durability continuous casting mold, and the effects of the temperature-controlled laser heat treatment on the variations of the surface mechanical properties and the microstructure were investigated.

2. Materials and Methods

2.1. Materials

A single type of commercial Stellite-1 (Deloro, Koblenz, Germany) powder was employed in the HVOF spraying. It was spherical shape (diameter: 30–45 μm) and the chemical composition is listed in Table 1. The substrate subjected to the thermal spraying consisted of two layers: a pure Cu sheet on which a pure Ni layer is deposited by electroplating. A schematic cross-sectional view of the substrate along with its dimensions is shown in Figure 1a.

Table 1. Chemical compositions of Stellite-1 powder used (wt.%).

Materials	Co	Cr	C	W	Ni	Si	Fe	Mo
Stellite-1	Bal.	31	2.5	12	3.0	2.0	3.0	1.0

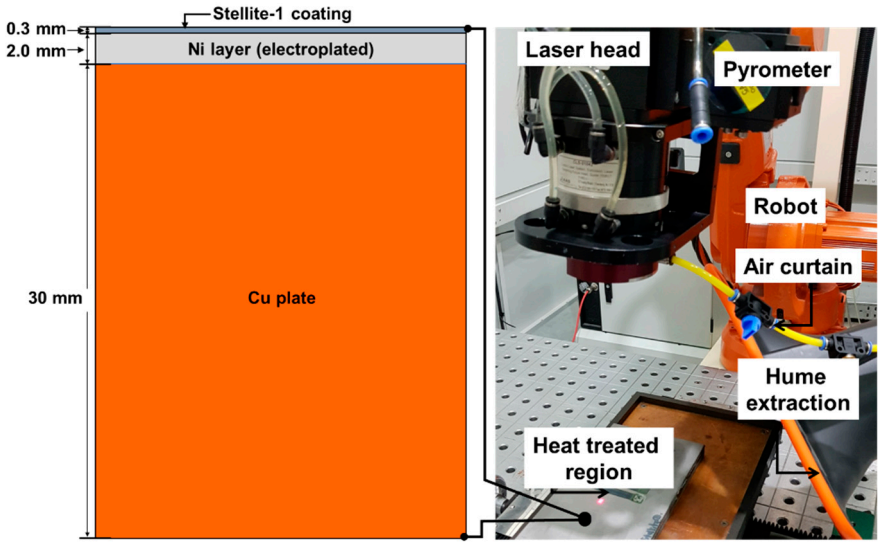

Figure 1. Schematic description of the specimen and the overall view of the experimental setup for laser heat treatment.

2.2. Experimental Procedures

The pure Cu sheet was electroplated with pure Ni. Next, thermal spraying of the substrate (i.e., spraying carried out on the surface of the electroplated pure Ni layer) was performed using the HVOF method. The thermal spraying conditions are summarized in Table 2. The specimens were then subjected to heat treatment using a diode laser system. The key conditions for the laser heat treatment are listed in Table 3, while Fig. 1 also shows the laser heat treatment experiment and the arrangement of the specimen. The laser beam dimensions were 6 mm × 4 mm. Laser beam irradiation was performed with temperature control applied in real time. The incident laser power was automatically controlled to regulate the temperature. To this end, in order to monitor the heat treatment temperature at the specimen surface, a pyrometer was positioned coaxially with the laser beam. The laser head, together with the pyrometer system, was controlled by a multi-axis robot. The heat treatment was performed over a temperature range of 1373–1473 K, at a laser scan speed of 0.5 mm/s.

Table 2. Conditions of HVOF coating.

Parameter	Value
Thermal sprayer	JP-5000®
Powder flow rate (g/m)	70–100
Oxygen flow rate (ℓ/m)	1000–1200
Gasoline flow rate (ℓ/m)	3–5
Thickness of sprayed layer (mm)	0.3

The cross-sectional macrostructure of the treated specimen was observed using optical microscopy (OM, BX51M, Olympus, Tokyo, Japan). X-ray diffraction (XRD, Ultima IV, Rigaku, Tokyo, Japan) with Cu-Kα radiation was used to qualitatively identify the phase variation after the laser heat treatment of the coating layer. The diffraction data were collected over a 2θ range of 30–80°. The cross-sectional microstructure and the elemental distribution were observed and analyzed using scanning electron microscopy (SEM, JXA-8530F, JEOL, Tokyo, Japan) and electron probe X-ray micro

analysis (EPMA, JXA-8530F, JEOL). The metallographic samples were prepared by polishing until 1 μm. The characterization of phases was performed by a transmission electron microscope (TEM, JEM-2100F, JEOL) with an energy-dispersive X-ray spectroscope (EDS, Inca X-sight, Oxford Instrument, Oxford, UK). TEM samples were prepared using a multi-beam focused-ion beam (FIB) and a scanning electron microscope (SEM) system (LYRA 1 XMH, Tescan, Kohoutovice, Czech), using an in-situ lift-out method. To confirm the effect of the heat treatment conditions on the mechanical properties of the thermal spray coating, Vickers hardness testing (MMT-X, Matsuzawa, Akita, Japan) was performed with a testing load of 25 gf and a dwell time of 10 s. The hardness was evaluated on three layers within the cross-sectional coating (top: below 0.05 mm, middle: below 0.15 mm, bottom: below 0.25 mm from the coating surface), and the measurement width and interval was 5 mm (within the heat-treated region) and 0.2 mm, respectively. The influence of the laser heat treatment on the tribological properties of the coating were also evaluated by a pin-on-disk tribometer (CETR UMT-2, Bruker, Billerica, MA, USA). The 10 mm × 10 mm × 8 mm sized samples were pressed against a rotating cast iron disk with a diameter of 142 mm. All the samples were burnished before the tribology testing to achieve an even surface contact with a counter material. The burnishing process was conducted with SiC abrasive papers (PC221, # 600 mesh size Deerfos Co., Seoul, Korea) attached to the cast iron disk. The tribological properties of as-sprayed and laser heat-treated samples were measured by sliding them against SiC abrasive papers (PC221, # 320 mesh size, Deerfos Co.) attached to the cast iron disk. The new SiC abrasive paper was utilized at every 30 m of sliding distance. The tribotesting was conducted using 30 N of normal load, 28.8 mm/s of sliding speed, and 120 m of total wear distance. At every 30 m of wear distance, the worn volume was measured to calculate the wear rate. The average roughness of the worn surface was measured by laser microscopy (VK-8710, Keyence, Osaka, Japan) after the tribotesting.

Table 3. Specification of equipment and conditions for laser surface heat treatment.

Parameter	Value
Oscillator	4 kW (capable maximum power) diode laser
Wavelength of laser beam (nm)	970
Beam dimensions (mm)	6 × 4 (square type)
Direction of laser beam irradiation	Perpendicular to specimen
Focal length (mm)	310
Defocus distance (mm)	0
Scan speed of laser beam (mm/s)	0.5
Homogenization temperature (K)	1373–1473

3. Selection and Control of Laser Heat Treatment Conditions

3.1. Thermodynamic Calculation of Phase Fraction

Figure 2 shows the relationship between the temperature (ranging from 1300 to 1550 K) and the phase fraction calculated for the Stellite-1 alloy using the Thermo-Calc software (TCNI8 database). The primary matrix phase within this temperature range comprised FCC-Co with HCP-Co; carbides were also confirmed to be present in the secondary phase. The temperature range selected for this study included temperatures at which the material would exist in the solid state (i.e., 1373, 1423, and 1473 K). The treatment temperature is also indicated in Figure 2.

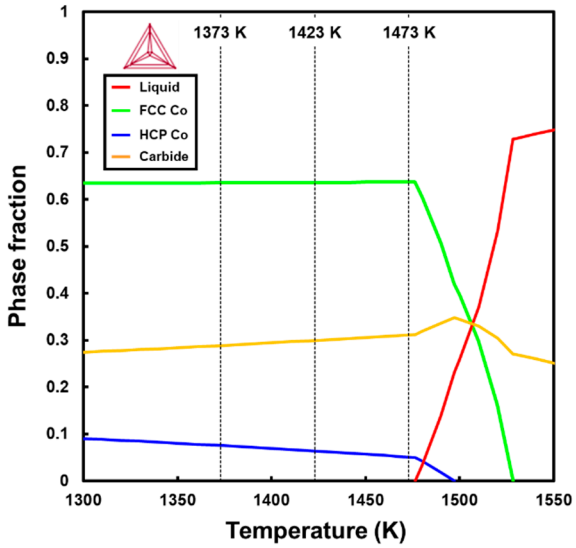

Figure 2. Relationship between the phase fraction and temperature for Stellite-1.

3.2. History of Surface Temperature and Laser Power during Laser Irradiation

Figure 3 shows the representative surface temperature and laser power trends during the laser heat treatment at 1473 K. The target heat treatment temperature was consistently maintained by adjusting the laser power in real time. The laser power was approximately 0.9 kW at the beginning of the heat treatment, and was later decreased to a stable value of 0.6 kW (approximately) at the heat treatment temperature of 1473 K. Similar temperature and laser power trends were observed for other heat treatment conditions.

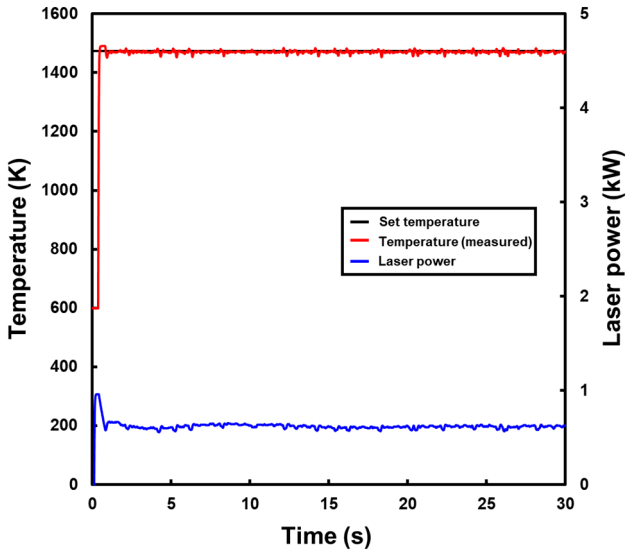

Figure 3. Trends for the laser power and temperature against time during laser heat treatment (set temperature: 1473 K).

4. Macro- and Microstructure of the As-Sprayed Coating

Figure 4 shows the representative cross-sectional OM and SEM (backscattered electron (BSE) mode) images for the as-sprayed Stellite-1 coating. As shown in Figure 4a, the HVOF sprayed coating covered the electroplated Ni layer, and large numbers of voids were present within the coating. The SEM micrograph (image of "Enlarged A") demonstrates that the microstructure of the as-sprayed coating consisted of individual splats. In the splats, the dendritic structure could be recognized and the voids were mainly positioned in the intersplat boundaries.

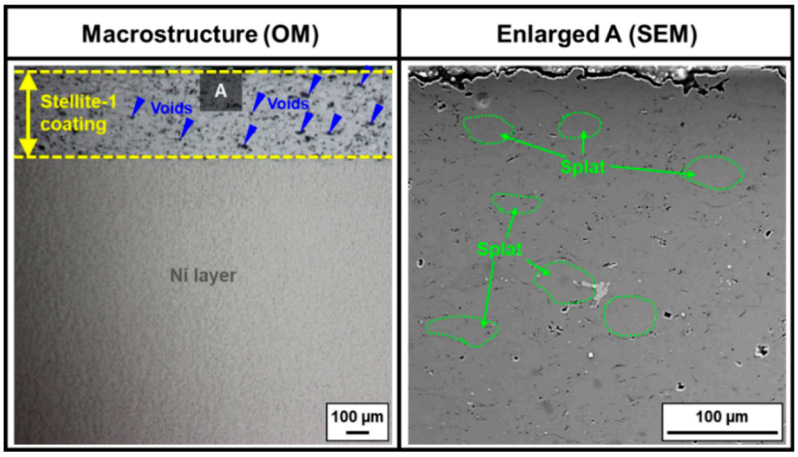

Figure 4. Cross-sectional OM and SEM (backscattered electron mode) micrographs of the as-sprayed Stellite-1 coating.

Figure 5a shows the BSE images and the distribution maps of the alloying elements for the as-sprayed coating analyzed by EPMA and Figure 5b also shows the enlarged view and corresponding distribution at the region "A" marked in Figure 5a. A slight macrosegregation of certain elements such as Si, Mo, and W was observed in the corresponding distribution maps in Figure 5a. Furthermore, as displayed in Figure 5b, no carbides (i.e., W- or Cr-based carbides) were present.

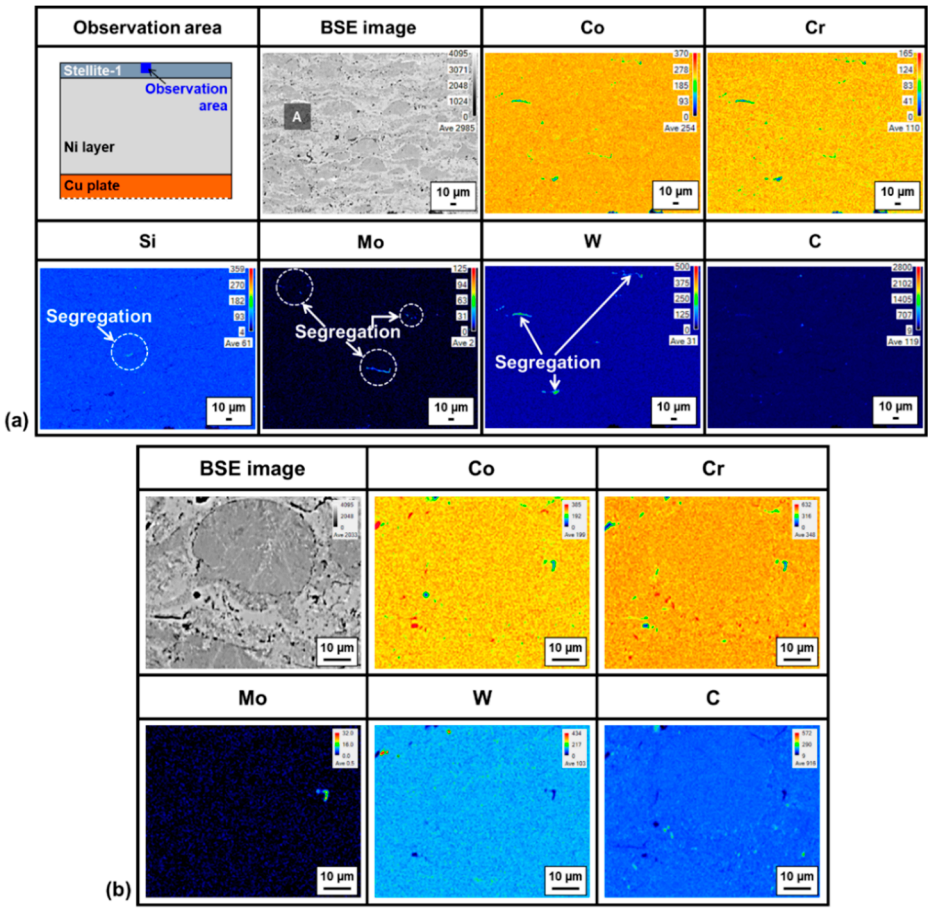

Figure 5. (**a**) Element distribution and BSE images of the as-sprayed Stellite-1 coating obtained by EPMA, and (**b**) enlarged view and corresponding element distributions in region "A" in (**a**).

5. Variation of Macrostructure and Hardness by Laser Heat Treatment

5.1. Cross-Sectional Macrostructure

Figure 6 shows the variations in the cross-sectional optical macrostructure as a function of the heat treatment temperature for the Stellite-1 coating. It was confirmed that the number of voids within the as-sprayed coating decreased slightly in number with an increase in the temperature from the macrostructural viewpoint. At the heat treatment temperature of 1473 K, the Stellite-1 coating was almost homogenized.

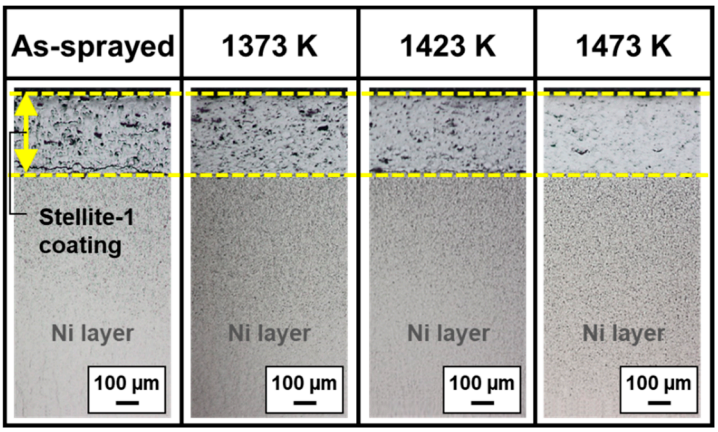

Figure 6. Cross-sectional macrostructures as functions of the heat treatment temperatures.

5.2. Hardness Variation

Figure 7 shows the hardness variation upon being subjected to laser heat treatment temperatures. The position and interval of hardness measurement was also schematically depicted in Figure 7.

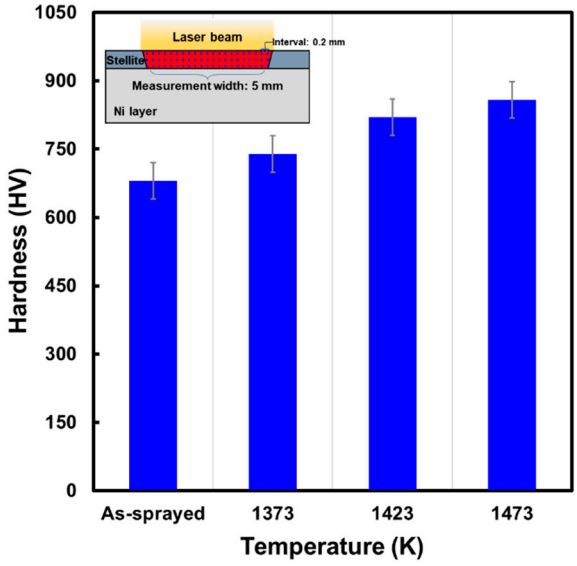

Figure 7. Relationship between laser heat treatment temperatures and the average hardness of Stellite-1 coating.

The average hardness value from the mapping was used in Figure 7. The hardness of the Stellite-1 coating increased from the level observed with the as-sprayed coating (680 HV) to that observed with the heat-treated coating at 1473 K (860 HV). In other words, approximately 130% of the hardness increment could be attributed to the laser heat treatment of the Stellite-1 coating. Figure 8 shows the typical XRD

patterns obtained for the as-sprayed coating and the laser heat-treated coatings. The formation of the M_7C_3, $M_{23}C_6$, and WC phases was attributed to the laser heat treatment by comparing the XRD patterns obtained for the laser heat treated coatings and those for the plain as-sprayed coatings. We speculate that 130% of the hardness increment is highly related to the formation of these secondary phases. The formation of the M_7C_3, $M_{23}C_6$, and WC phases was confirmed for the laser heat-treated Stellite-1 coating, and these secondary phases induced the increase in hardness after the laser heat treatment.

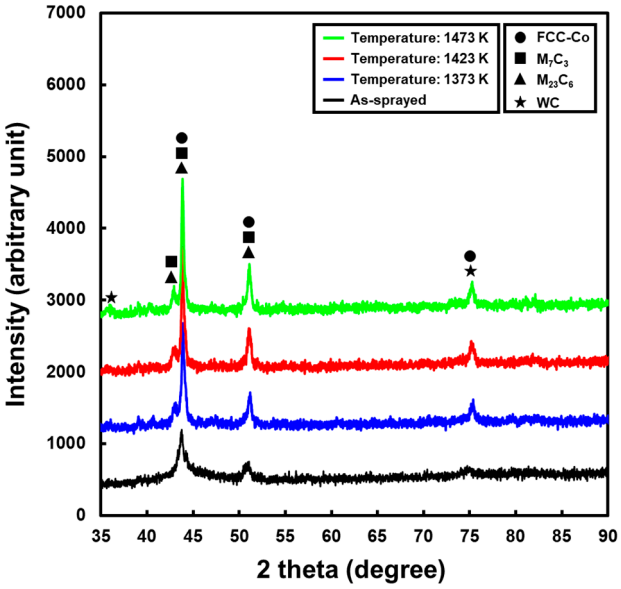

Figure 8. XRD patterns obtained for the as-sprayed Stellite-1 coating and laser heat-treated coating.

6. Relationship between Hardness and Microstructural Features

Figure 9a shows the backscattered electron (BSE) image and distribution maps of the alloying elements analyzed by EPMA near the surface of the laser heat-treated Stellite-1 coating at 1373 K. Figure 9b shows the enlarged views and corresponding distribution for the region "A" marked in Figure 9a. In Figure 9a, it can be clearly observed that the intersplat boundaries weakened and the extent of the void decreased—that is, the inhomogeneity of the as-sprayed coating was enhanced near the surface because of the laser heat treatment as compared to that of the as-sprayed coating without the treatment (Figures 4 and 5). This enhancement occurred despite the presence of the macrosegregation of certain alloying elements (such as Co and W). Based on the BSE image, the depth of the heat-treated region was approximately 130 μm at 1373 K of heat treatment temperature. In addition, in the enlarged view in Figure 9b, the formation of secondary phases such as W- and Cr-based carbides can be observed that are not seen in the as-sprayed coating without laser heat treatment (Figure 5b). Figure 10 also shows the BSE images and distribution maps for the alloying elements analyzed by EPMA near the surface of the laser heat-treated Stellite-1 coating at 1473 K (heat treatment condition giving the highest hardness). The splat structures, the segregation of certain elements, and the voids were diminished. Furthermore, the microstructure of the sprayed coating fully consisted of fine secondary phases based on the Co matrix. These secondary phases were also W- and Cr-based carbides.

Figure 11 displays representative bright field (BF) image and energy dispersive X-Ray spectroscopy (EDS) results analyzed by TEM for the laser heat-treated Stellite-1 coating at 1473 K. Similar to the results obtained by EPMA (Figure 10), the carbides consisted of W and Cr and their size distributions ranged from 30 to 300 nm. Figure 12 also shows the BF image and elected area diffraction pattern (SADP) of the carbides. The matrix phase was FCC-structured Co (SADP-A in Figure 12a) and the carbides could be characterized by M_7C_3 (SADP-B in Figure 12a), WC (SADP-C in Figure 12b), and $M_{23}C_6$ (SADP-D in Figure 12b). These characterization results coincide well with those obtained by the XRD pattern mentioned in Figure 8. It has been reported that a high hardness is mainly due to

the formation of Cr- and W-rich carbides and the solid solution hardening of W in the FCC-Co phase for Stellite-1 alloys [26]. Thus, the main reason for the increase in the hardness after the laser heat treatment as shown in Figure 7, could be the formation of these nano-sized WC, M_7C_3, and $M_{23}C_6$.

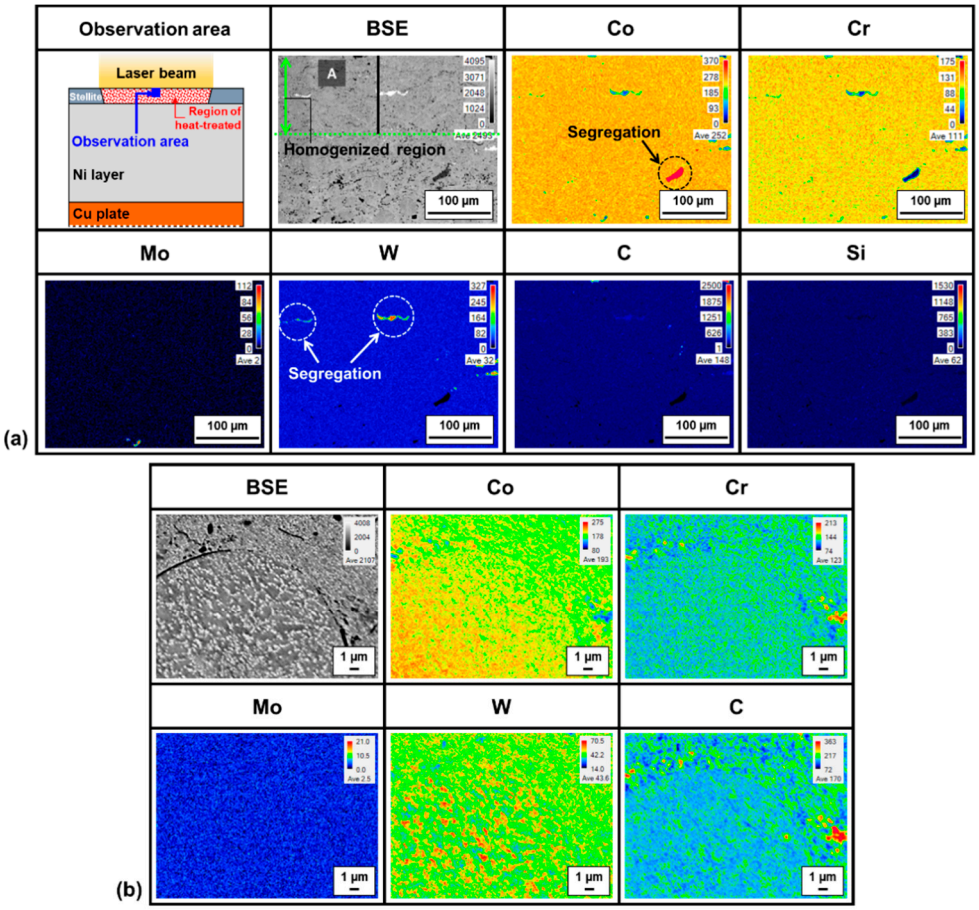

Figure 9. (**a**) Element distribution and (**b**) BSE images of Stellite-1 coating after laser heat treatment at 1373 K.

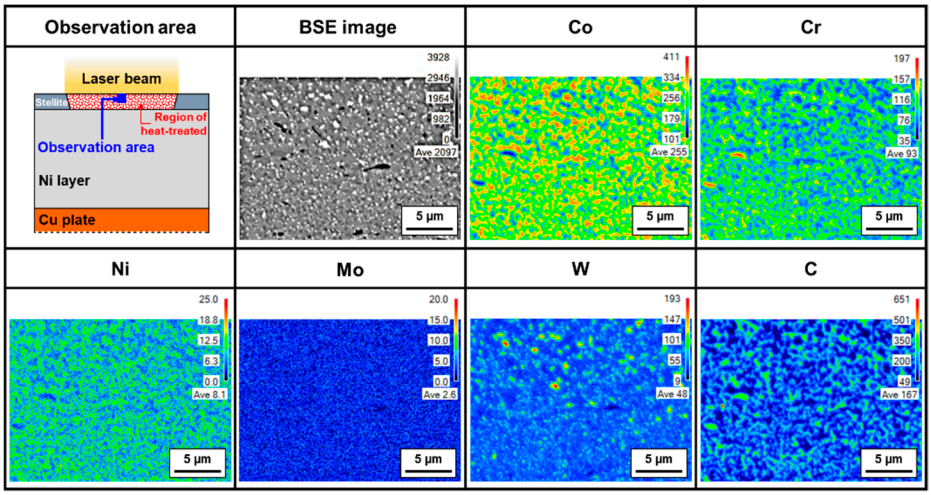

Figure 10. Element distribution and BSE images of the Stellite-1 coating after laser heat treatment at 1473 K.

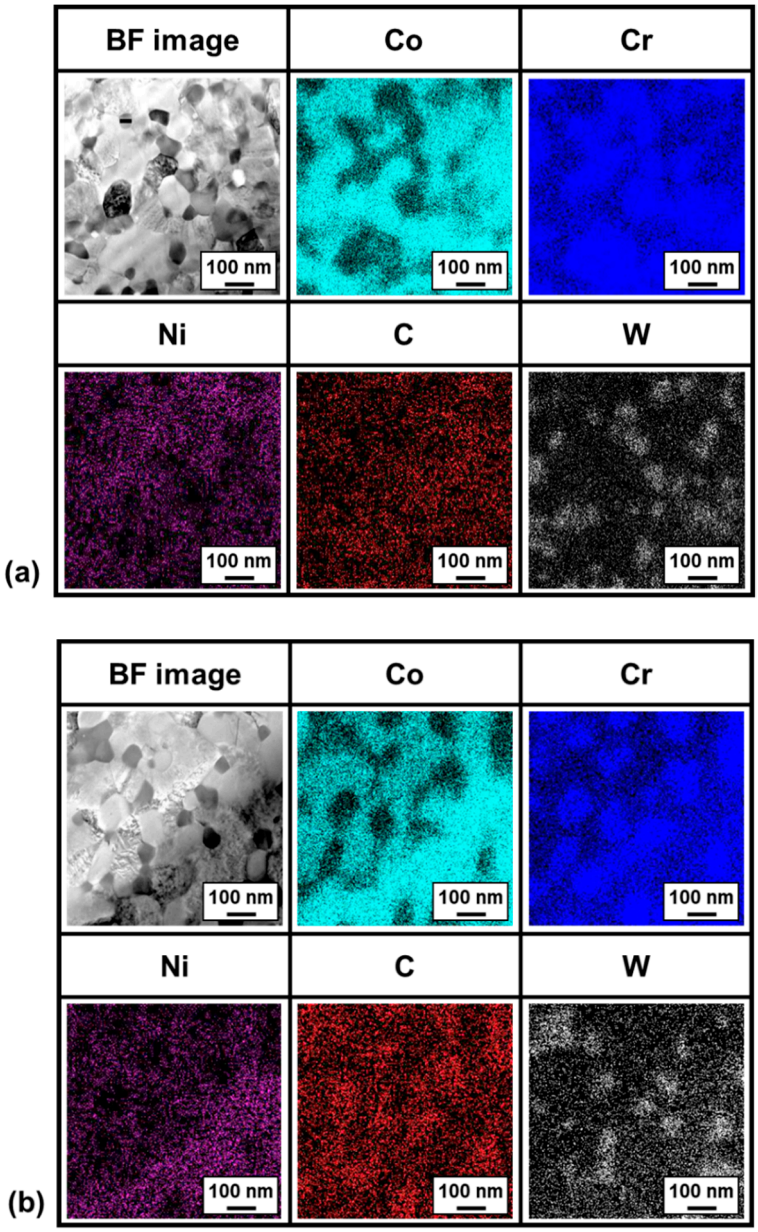

Figure 11. (**a**,**b**) BF images and EDS results of laser heat treated Stellite-1 coating at 1473 K.

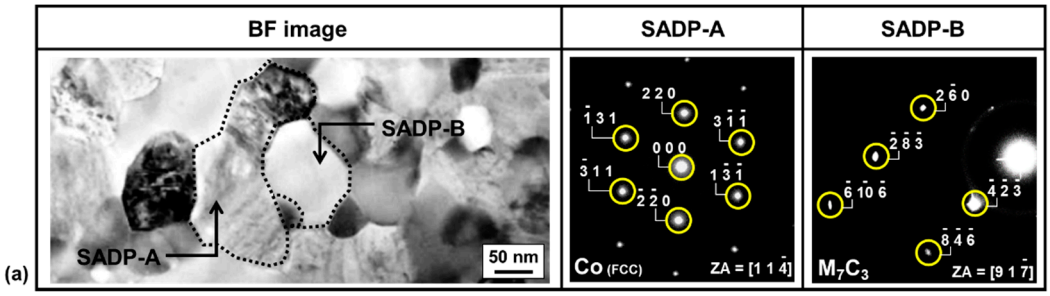

Figure 12. *Cont*.

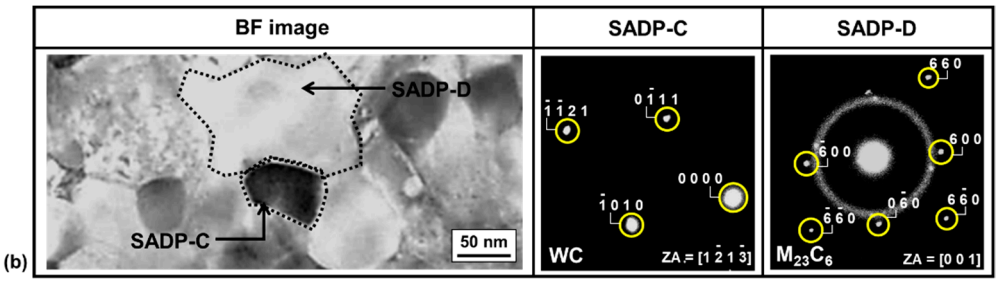

Figure 12. BF image and corresponding SADP for laser heat treated Stellite-1 coating at 1473 K: (**a**) Co and M_7C_3, (**b**) WC and $M_{23}C_6$.

7. Effect of Nano-Sized Carbides Formation and Surface Hardening on Tribological Properties

Figure 13 shows the coefficient of friction (COF) as a function of wear distance for the as-sprayed coating and laser heat-treated coating at 1473 K. The COF of the laser heat-treated coating was relatively lower than that of the as-sprayed coating. The average COF was found to be 0.419 for the as-sprayed coating and 0.296 for the laser heat-treated coating. The small COF of the laser heat-treated coating was attributed to the increase in hardness because of the formation of nano-sized Cr- and W-rich carbides after the laser heat treatment as mentioned in Figures 10 and 11.

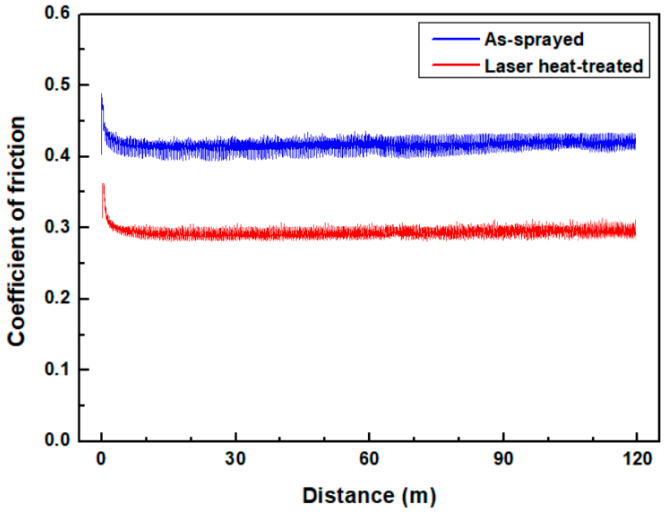

Figure 13. COF as a function of wear distance for the as-sprayed coating and laser heat-treated coating at 1473 K.

In addition, the variation in the COF of the laser heat-treated coating was relatively smaller in comparison to that in the as-sprayed coating. The difference between the maximum COF (COF_{max}) value and the minimum COF (COF_{min}) value was found to be 0.044 for the as-sprayed coating (COF_{max}: 0.436 and COF_{min}: 0.392). On the other hand, the difference between COF_{max} and COF_{min} was 0.034 for the laser heat-treated coating (COF_{max}: 0.314 and COF_{min}: 0.28). Small variations in COF for the laser heat-treated coating were attributed to microstructural homogeneity; that is, the laser heat treatment on the Stellite-1 coating reduced the number of macrosegregations and voids, resulting in uniform wear behavior. Figure 14 demonstrates the wear rate of as-sprayed and laser heat-treated coatings at every 30 m of wear distance. The wear rate at 120 m of wear distance was found to be 17.93×10^3 mm^3/Nm for the as-sprayed coating and 15.09×10^3 mm^3/Nm for the laser heat-treated coating. The wear rate of the laser heat-treated sample was 15.8% smaller than that of the as-sprayed sample. This result suggested that the wear resistance of the Stellite-1 coating was enhanced by the laser heat treatment. The SEM images in Figure 15 show the surface morphology of the as-sprayed and laser heat-treated coatings after the tribotesting. A relatively smoother surface morphology was detected in the laser

heat-treated sample than in the as-sprayed sample. In the case of the as-sprayed sample, deep and thick abrasion grooves, wear debris, and spalling were detected at the worn surface. The presented voids at the Stellite-1 coating may cause the surface damage in the form of spalling. On the other hand, thin and shallow abrasion grooves with small-sized debris were observed for the laser heat-treated sample. The measured average roughness (R_a) of the worn surface after the tribotesting was 3.79 μm for the as-sprayed sample and 2.83 μm for the laser heat-treated sample. The laser heat treatment on the Stellite-1 coating increased the surface hardness and microstructural homogeneity, resulting in an enhancement of wear resistance.

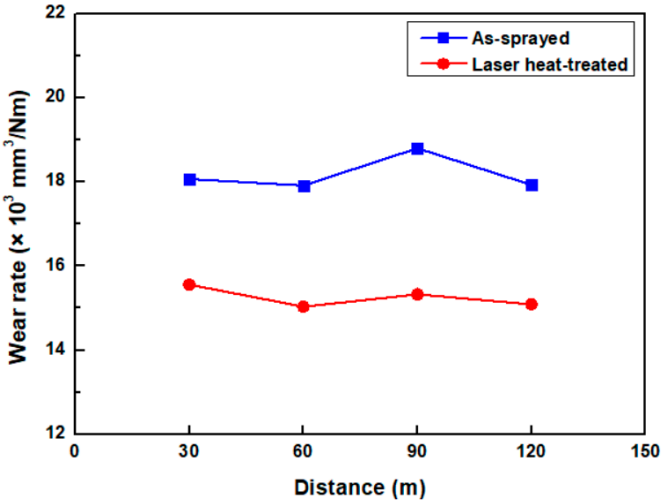

Figure 14. Measured wear rate of the as-sprayed coating and laser heat-treated coating at 1473 K at every 30 m of wear distance.

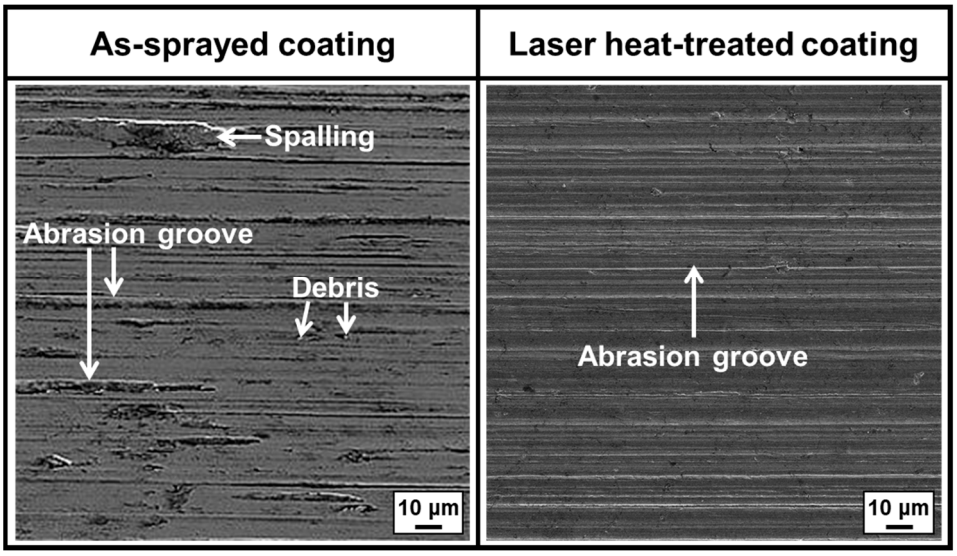

Figure 15. SEM image of the worn surface of an as-sprayed sample and the laser heat-treated sample at 1473 K after the tribotesting.

8. Conclusions

To develop high-durability continuous casting mold components, a Stellite-1 coating sprayed by the HVOF technique was subjected to the temperature-controlled laser heat treatment using a high-power diode laser. The effects of the heat treatment on macro- and microstructural variations in the coating along with the hardness distribution within the coating were investigated. In the as-sprayed Stellite-1 coating, large numbers of micro-voids and macrosegregation of certain alloying

elements existed. Furthermore, homogeneously distributed carbides could not be detected. After the laser heat treatment, voids within the sprayed coating decreased slightly with an increase in the macrostructural temperature. At the heat treatment temperature of 1473 K, the Stellite-1 coating was almost homogenized. The hardness of the sprayed Stellite-1 coating increased after the laser heat treatment from that of the as-sprayed coating (680 HV) to 860 HV at 1473 K. The hardness increment could be attributed to the formation of nano-sized W- and Cr-based carbides such as WC, M_7C_3, and $M_{23}C_6$, as suggested by TEM analysis. The effect of the laser heat treatment on the tribological properties of Stellite-1 coating was analyzed by a pin-on-disk tribotest. The laser heat-treated sample at 1473 K showed a smaller COF and wear rate than those of the as-sprayed sample. This result was attributed to the formation of nano-sized carbides on the Stellite-1 coating because of the laser heat treatment that caused surface hardening, resulting in an increment of wear resistance.

Author Contributions: Investigation, C.-K.P. and J.-H.L.; Writing—original draft, C.-K.P. and E.-J.C.; Writing—review & editing, N.-H.K. and E.-J.C.; Supervision, E.-J.C. All authors have read and agreed to the published version of the manuscript.

Funding: This work was supported by National Research Foundation, Korea (Project No. 2019R1G1A1099607) and the National Research Council of Science and Technology, Korea (Project No. NK227C, 2020).

Conflicts of Interest: The authors declare no conflict of interest.

References

1. Sassatelli, P.; Bolelli, G.; Gualtieri, M.L.; Heinonen, E.; Honkanen, M.; Lusvarghi, L.; Manfredini, T.; Rigon, R.; Vippola, M. Properties of HVOF-sprayed Stellite-6 coatings. *Surf. Coat. Technol.* **2018**, *338*, 45–62. [CrossRef]
2. Brownlie, F.; Hodgkiess, T.; Pearson, A.; Galloway, A.M. Effect of nitriding on the corrosive wear performance of a single and double layer Stellite 6 weld cladding. *Wear* **2017**, *376–377*, 1279–1285. [CrossRef]
3. Gholipour, A.; Shamanian, M.; Ashrafizadeh, F. Microstructure and wear behavior of Stellite 6 cladding on 17-4 PH stainless steel. *J. Alloy Compd.* **2011**, *509*, 4905–4909. [CrossRef]
4. Dilawary, S.A.A.; Motallebzadeh, A.; Afzal, M.; Atar, E.; Cimenoglu, H. Laser surface melting of 10 wt% Mo alloyed hardfacing Stellite 12 plasma transferred arc deposits: Structural evolution and high temperature wear performance. *Opt. Laser Technol.* **2018**, *101*, 404–412. [CrossRef]
5. Yao, J.; Li, Z.; Li, B.; Yang, L. Characteristics and bonding behavior of Stellite 6 alloy coating processed with supersonic laser deposition. *J. Alloy Compd.* **2016**, *661*, 526–534. [CrossRef]
6. Yao, J.; Ding, Y.; Liu, R.; Zhang, Q.; Wang, L. Wear and corrosion performance of laser-clad low-carbon high-molybdenum Stellite alloys. *Opt. Laser Technol.* **2018**, *107*, 32–45. [CrossRef]
7. Fallah, V.; Alimardani, M.; Corbin, S.F.; Khajepour, A. Impact of localized surface preheating on the microstructure and crack formation in laser direct deposition of Stellite 1 on AISI 4340 steel. *Appl. Surf. Sci.* **2010**, *257*, 1716–1723. [CrossRef]
8. Alimardani, M.; Fallah, V.; Khajepour, A.; Toyserkani, E. The effect of localized dynamic surface preheating in laser cladding of Stellite 1. *Surf. Coat. Tech.* **2010**, *204*, 3911–3919. [CrossRef]
9. Matthews, S.; James, B. Review of thermal spray coating applications in the steel industry: Part 1– hardware in steel making to the continuous annealing process. *J. Therm. Spray Technol.* **2010**, *19*, 1267–1276. [CrossRef]
10. Chen, H.; Su, L.; Wang, G.; Wan, S.; Zhang, L.; Luo, Z. Fuzzy estimation for heat flux distribution at the slab continuous casting mold surface. *Int. J. Therm. Sci.* **2014**, *83*, 80–88. [CrossRef]
11. Barella, S.; Gruttadauria, A.; Mapelli, C.; Mombelli, D. Investigation of failure and damages on a continuous casting copper mould. *Eng. Fail. Anal.* **2014**, *36*, 432–438. [CrossRef]
12. Sakata, K.; Nakano, K.; Miyahara, H.; Matsubara, Y.; Ogi, K. Microstructure control of thermally sprayed Co-based self-fluxing alloy coatings by diffusion treatment. *J. Therm. Spray Technol.* **2007**, *16*, 991–997. [CrossRef]
13. Houdkova, S.; Smazalova, E.; Pala, Z. Effect of heat treatment on the microstructure and properties of HVOF-sprayed Co-Cr-W coating. *J. Therm. Spray Technol.* **2016**, *25*, 546–557. [CrossRef]
14. Ciubotariu, C.R.; Frunzaverde, D.; Marginean, G.; Serban, V.A.; Birdeanu, A.V. Optimization of the laser remelting process for HVOF-sprayed Stellite 6 wear resistant coatings. *Opt. Laser Technol.* **2016**, *77*, 98–103. [CrossRef]

15. Houdkova, S.; Pala, Z.; Smazalova, E.; Vostrak, M.; Cesanek, Z. Microstructure and sliding wear properties of HVOF sprayed, laser remelted and laser clad Stellite 6 coatings. *Surf. Coat. Technol.* **2017**, *318*, 129–141. [CrossRef]
16. Vostrak, M.; Tesar, J.; Houdkova, S.; Smazalova, E.; Hruska, M. Diagnostic of lase remelting of HVOF sprayed Stellite coatings using an infrared camera. *Surf. Coat. Tech.* **2017**, *318*, 360–364. [CrossRef]
17. Gil, L.; Prato, M.A.; Staia, M.H. Effect of post-heat treatment on the corrosion resistance of NiWCrBSi HVOF coatings in chloride solution. *J. Therm. Spray Technol.* **2002**, *11*, 95–99. [CrossRef]
18. Navas, C.; Colaco, R.; Damborene, J.D.; Vilar, R. Abrasive wear behaviour of laser clad and flame sprayed-melted NiCrBSi coatings. *Surf. Coat. Technol.* **2006**, *200*, 6854–6862. [CrossRef]
19. Bolelli, G.; Lusvarghi, L.; Barletta, M. Heat treatment effects on the corrosion resistance of some HVOF-sprayed metal alloy coatings. *Surf. Coat. Technol.* **2008**, *202*, 4839–4847. [CrossRef]
20. Suutala, J.; Tuominen, J.; Vuoristo, P. Laser-assisted spraying and laser treatment of thermally sprayed coatings. *Surf. Coat. Technol.* **2006**, *201*, 1981–1987. [CrossRef]
21. Chun, E.J.; Kim, M.S.; Nishikawa, H.; Park, C.; Suh, J. Laser-assisted selective fusing of thermal sprayed Ni-based self-fluxing alloys by using high-power diode lasers. *Opt. Laser Technol.* **2018**, *100*, 317–324. [CrossRef]
22. Zhang, S.H.; Yoon, J.H.; Li, M.X.; Cho, T.Y.; Joo, Y.K.; Cho, J.Y. Influence of CO_2 laser heat treatment on surface properties, electrochemical and tribological performance of HVOF sprayed WC–24%Cr_3C_2–6%Ni coating. *Mater. Chem. Phys.* **2010**, *119*, 458–464. [CrossRef]
23. Gonzalez, R.; Garcia, M.A.; Penuelas, I.; Cadenas, M.; Fernandez, M.D.R.; Battez, A.H.; Felgueroso, D. Microstructural study of NiCrBSi coatings obtained by different processes. *Wear* **2007**, *263*, 619–624. [CrossRef]
24. Gonzalez, R.; Cadenas, M.; Fernandez, R.; Cortizo, J.L.; Rodriguez, E. Wear behaviour of flame sprayed NiCrBSi coating remelted by flame or by laser. *Wear* **2007**, *262*, 301–307. [CrossRef]
25. Lugscheider, E.; Hofmann, D.; Nicoll, A.R. Optimization of spraying process and laser treatment of CoNiCrAlY. *J. Therm. Spray Technol.* **1992**, *1*, 239–247. [CrossRef]
26. Frenk, A.; Kurz, W. Microstructural effects on the sliding wear resistance of a cobalt-based alloy. *Wear* **1994**, *174*, 81–91. [CrossRef]